

## Trace Gas/Aerosol Boundary Concentrations and their Impacts on Continental-Scale AQMEII Modeling Domains

Kenneth Schere<sup>a\*</sup>, Johannes Flemming<sup>b</sup>, Robert Vautard<sup>c</sup>, Charles Chemel<sup>d,e</sup>, Augustin Colette<sup>f</sup>, Christian Hogrefe<sup>g</sup>, Bertrand Bessagnet<sup>f</sup>, Frederik Meleux<sup>f</sup>, Rohit Mathur<sup>a</sup>, Shawn Roselle<sup>a</sup>, Rong-Ming Hu<sup>e</sup>, Ranjeet S. Sokhi<sup>e</sup>, S.T. Rao<sup>a</sup>, Stefano Galmarini<sup>h</sup>

<sup>a</sup>Atmospheric Modeling and Analysis Division, National Exposure Research Laboratory, Office of Research and Development, US Environmental Protection Agency, Research Triangle Park, NC 27711, USA

<sup>b</sup>European Centre for Medium-Range Weather Forecasts (ECMWF), Reading, UK

<sup>c</sup>Laboratoire des Sciences du Climat et de l'Environnement, IPSL, CEA/CNRS/UVSQ, Gif/Yvette, FRANCE

<sup>d</sup>National Centre for Atmospheric Science (NCAS), Centre for Atmospheric & Instrumentation Research (CAIR), University of Hertfordshire, Hatfield, UK

<sup>e</sup>Centre for Atmospheric & Instrumentation Research (CAIR), University of Hertfordshire, Hatfield, UK

<sup>f</sup>Institut National de l' Environnement Industriel et des Risques (INERIS), Parc Technologique Alata, Verneuil en Halatte, FRANCE

<sup>g</sup>Bureau of Air Quality Analysis and Research, New York State Department of Environmental Conservation, Albany, NY 12233, USA

<sup>h</sup>European Commission-Joint Research Center, Institute for Environment and Sustainability, I-21027 Ispra, ITALY

\*Corresponding author: Tel: +01-919-5413795; fax: +01-919-5411379. E-mail: [schere.kenneth@epa.gov](mailto:schere.kenneth@epa.gov). U.S. EPA-E243-04, Research Triangle Park, NC 27711 USA

(Submitted to Atmospheric Environment: 6 May 2011)

1 **Abstract**

2  
3  
4  
5  
6  
7  
8  
9  
10  
11  
12  
13  
14  
15  
16  
17  
18  
19  
20  
21  
22  
23  
24  
25  
26  
27  
28  
29

Over twenty modeling groups are participating in the Air Quality Model Evaluation International Initiative (AQMEII) in which a variety of mesoscale photochemical and aerosol air quality modeling systems are being applied to continental-scale domains in North America and Europe for 2006 full-year simulations for model inter-comparisons and evaluations. To better understand the reasons for differences in model results among these participating groups, each group was asked to use the same source of emissions and boundary concentration data for their simulations. This paper describes the development and application of the boundary concentration data for this AQMEII modeling exercise. The European project known as GEMS (Global and regional Earth-system Monitoring using Satellite and in-situ data) has produced global-scale re-analyses of air quality for several years, including 2006 (<http://gems.ecmwf.int>). The GEMS trace gas and aerosol data were made available at 3-hourly intervals on a regular latitude/longitude grid of approximately 1.9-degree resolution within 2 “cut-outs” from the global model domain. One cut-out was centered over North America and the other over Europe, covering enough spatial domain for each modeling group to extract the necessary time- and space-varying (horizontal and vertical) concentrations for their mesoscale model boundaries. Examples of the impact of these boundary concentrations on the AQMEII continental simulations are presented to quantify the sensitivity of the simulations to boundary conditions. In addition, some participating groups were not able to use the GEMS data and instead relied upon other sources for their boundary concentration specifications. These are noted, and the contrasting impacts of other data sources for boundary data are presented. How one specifies four-dimensional boundary concentrations for mesoscale air quality simulations can have a profound impact on the model results, and hence, this aspect of data preparation must be performed with considerable care.

Keywords: air quality modeling, boundary concentrations, model evaluation, AQMEII, GEMS

30 **1. Introduction**

31

32 The evaluation of regional- through continental-scale photochemical and aerosol air quality  
33 simulation modeling systems (PAQMs) has been a subject of considerable interest in recent  
34 years (Dennis et al., 2010; Vautard et al., 2007; McKeen et al., 2005). Such systems have been  
35 adopted by the air quality management and forecasting communities to provide estimates of  
36 future (10 years and longer) air quality based on planned emissions mitigation actions, as well as  
37 forecasts of short-term (1-3 days) air quality for public notice and alerts (Honoré et al., 2009;  
38 Eder et al., 2010). The results from these model applications have become increasingly visible  
39 and significant from the standpoint of public perceptions as well as having considerable  
40 economic, political, and social implications. Therefore, it is necessary that users of the models  
41 and consumers of the model results have sufficient confidence in these tools and their predictions  
42 to use for the intended applications. Such confidence can be obtained, in part, from evaluations  
43 of the models against real-world measurements for their particular applications.

44 To better foster a structured and coordinated approach to the PAQM evaluations at the  
45 international level, an Air Quality Model Evaluation International Initiative (AQMEII) was  
46 launched in 2008 as a collaboration between North American and European modeling groups  
47 (Rao et al., 2011; <http://aqmeii.jrc.ec.europa.eu>). AQMEII is aimed at providing a permanent  
48 forum to constantly monitor the state of advancement of regional-scale PAQMs and model  
49 evaluation methodologies through the organization of periodic workshops and modeling  
50 activities in which the different aspects of model performance evaluation are considered. In the  
51 first phase of AQMEII, an initial exercise has been launched in which more than twenty  
52 modeling groups in North America and Europe are using their regional-scale PAQMs to simulate  
53 a full-year (2006) retrospective continental application. Each participating group has been  
54 requested to model both continents using common reference model input data sets, namely the  
55 gridded source emissions and the lateral boundary concentrations for each continent. The focus  
56 of the study is on the application of the structured model evaluation framework discussed in  
57 Dennis et al. (2010) to these model simulation results, using a comprehensive observational  
58 database consisting of surface, aircraft, and satellite data for model evaluation and model inter-  
59 comparison.

60 This paper describes the development of a set of prescribed boundary concentrations for each  
61 continental model domain for use by all AQMEII modelers for this exercise, as well as some of  
62 the major impacts of these boundary concentrations on model results. Regional- or even  
63 continental-scale geographical extents of modeling domains require careful specification of the  
64 vertical and horizontal profiles of boundary concentrations since typical airflows over North  
65 America and Europe can traverse each continent in a few days to a week. The trace gas and  
66 aerosol concentrations as specified at the model's boundaries will affect the model simulation  
67 results as this material is transported into the simulation domains and interacts with the model's  
68 internal processing of emissions, chemical transformations, deposition, etc. For this AQMEII  
69 exercise the minimum spatial extent of each continent to be modeled by all participants is  
70 defined by latitude/longitude boundaries:

71 North America: Latitude: 25.5°N to 58.5°N Longitude: 130°W to 59.5°W

72 Europe: Latitude: 35.0°N to 70.0°N Longitude: 15.0°W to 35°E

73 (See Figures 1 and 2 in Rao et al., 2011.)

74

## 75 **2. GEMS Re-analysis**

76

77 A variety of sources is used to specify boundary concentrations for retrospective regional-  
78 scale PAQM simulations. Ideally, observational data should be of sufficient density and quality  
79 to provide these specifications. However, model domain boundaries are often over the ocean or  
80 sparsely-monitored land areas. Satellite-based platforms provide data for only a few chemical  
81 species and only intermittently in space and time. Global-scale PAQMs of coarser resolution are  
82 another source for providing boundary concentrations to regional-scale models. For the  
83 AQMEII project, a combination of global-scale models with assimilation of satellite-based  
84 observational data was used to derive boundary concentrations. This hybrid analysis using  
85 model and observational data for a retrospective assessment is commonly referred to as “re-  
86 analysis”. In this case, data were derived from a multi-year re-analysis that included the target  
87 year of 2006 from the European Union-funded project of Global and regional Earth-system  
88 Monitoring using Satellite and in-situ data (GEMS; <http://gems.ecmwf.int>; Hollingsworth et al.,  
89 2008; GEMS, 2010).

90 The GEMS project was set up by thirty-one participating institutions coordinated by the  
91 European Centre for Medium-Range Weather Forecasts (ECMWF) to build and demonstrate the  
92 core capability for providing a comprehensive range of services related to the chemical and  
93 particulate matter composition of the atmosphere. Among the demonstrated capabilities were  
94 data analyses and modeling systems for monitoring global distributions of atmospheric  
95 constituents, with focus areas of climate, air quality, and ultraviolet radiation, especially as they  
96 affect European communities. Global re-analysis products from GEMS are available for the  
97 period 2003-2008. These re-analyses make use of satellite observations allowing the retrieval of  
98 O<sub>3</sub>, CO, CH<sub>4</sub>, CO<sub>2</sub>, and aerosol optical depth during the AQMEII period of interest. Although  
99 GEMS is now concluded, the work conducted therein is being extended and improved through  
100 the new Monitoring Atmospheric Composition and Climate project (MACC; [http://www.gmes-](http://www.gmes-atmosphere.eu)  
101 [atmosphere.eu](http://www.gmes-atmosphere.eu)).

102 Figure 1 illustrates the principal components of the GEMS global modeling system. The  
103 GEMS system was built within and around the ECMWF Integrated Forecasting System (IFS;  
104 <http://www.ecmwf.int/research/ifsdocs/>), a global operational weather forecasting model system,  
105 including the capability for four-dimensional variational data assimilation (Rabier et al., 2000).  
106 The IFS system is coupled with one of three global chemical transport models (CTMs):  
107 MOZART3 (Kinnison et al., 2007), MOCAGE (Bousserez et al., 2007), or TM5 (Huijnen et al.,  
108 2010) through a special-purpose OASIS4 software coupler (Flemming et al., 2009). The main  
109 idea behind the coupled system is that the IFS computes only the transport of the assimilated  
110 reactive gases while the tendencies due to chemical conversion, deposition and emission  
111 injection are provided by one of the CTMs. The simulation of global aerosol and greenhouse  
112 gases is directly included within the IFS model (Morcrette et al., 2009). In this way, the IFS  
113 needs to handle only five additional chemical tracers, while the comprehensive schemes of the  
114 CTMs contain between 55 and 118 gaseous species. The coupled CTM is driven by  
115 meteorological data from the IFS with a coupling frequency of one hour. For the AQMEII  
116 application, it is principally the IFS-MOZART3 configuration whose data has been processed for  
117 regional-scale model boundary concentrations.

118 The IFS uses a T159 spectrally-resolved global grid with a horizontal grid box size of about  
119 125 km. MOZART-3 uses a regular latitude/longitude grid of 1.875°x1.875°. The coupler  
120 performs horizontal bi-linear interpolations between the meteorological and CTM horizontal

121 grids. The vertical coordinate is given by 60 hybrid-sigma pressure levels, with a model top at  
122 0.1hPa. The same vertical coordinate is used by the IFS and all CTMs in the GEMS system to  
123 avoid the need for vertical interpolations. The coupling interval is 3600 s which is the largest  
124 acceptable time step for the IFS at a T159 resolution. Output is saved at 3-h intervals from the  
125 model simulations. Source emissions for the MOZART-3 global simulations are specified as  
126 monthly averages for a base year of 2000 for anthropogenic trace gases (RETRO database;  
127 Schultz et al., 2009) and aerosols (EDGAR, <http://www.pbl.nl/en/themasites/edgar/index.html>;  
128 SPEW, Bond et al., 2004). Eight-day average fire emissions for the 2006 model application year  
129 are derived from the Global Fire Emissions Database (GFEDv2; van der Werf et al., 2006).  
130 Biogenic, sea salt, and dust emissions are parameterized within the model based on  
131 meteorological inputs (GEMS, 2010).

132 The advantage of using the GEMS re-analysis data to provide boundary concentrations for  
133 AQMEII simulations compared to other global model outputs is that the GEMS results include  
134 the assimilation of observed data derived from satellite platforms. Figure 2 indicates the satellite  
135 data usage during the GEMS project, with the AQMEII target year of 2006 highlighted. There  
136 were multiple instruments available for measuring portions of the ozone (O<sub>3</sub>) column during  
137 2006, including from SCIAMACHY, SBUV-2, and MLS instruments. Taken together these data  
138 provide some vertical resolution to the O<sub>3</sub> column, with greatest fidelity in the stratosphere and  
139 upper troposphere (Flemming et al., 2011). In addition, CO columns are available from the  
140 MOPITT instrument, and aerosol optical depths (AODs) are derived from the MODIS  
141 instruments onboard the Terra and Aqua satellites. Information on atmospheric aerosols can be  
142 derived from the AOD retrievals. Complete details on the data assimilation system and  
143 implementation for GEMS can be found in Benedetti et al., 2009 and Inness et al., 2009.

144 The GEMS re-analysis outputs for 2006 were further processed by ECMWF for AQMEII use  
145 by interpolating all requested data for selected variables at 3-h intervals on a regular  
146 latitude/longitude (1.875°X1.875°) grid within specific geographical “cut-outs” from the global  
147 model domain. These cut-outs for Europe and for North America are illustrated in Figure 3. The  
148 spatial extent of each cut-out extends well beyond the minimum domain sizes specified for  
149 AQMEII regional/continental domains such that AQMEII participants could use the data within  
150 the global cut-outs to derive the boundary concentrations for their own model exercises. Data  
151 from the lowest 47 IFS model layers (surface through 10hPa) were extracted within each cut-out

152 over a full time period of 1 December 2005 through 31 December 2006, allowing for sufficient  
153 model spin-up time for the 2006 simulation. Table 1 lists the chemical and aerosol species  
154 extracted for AQMEII use. These data were archived and made available to AQMEII  
155 participants by collaborators in Météo-France.

156 Air quality modelers participating in AQMEII then are able to access these GEMS data and  
157 use them for specification of boundary concentrations. There are, however, additional  
158 assumptions and processing steps involved before the data can be used by the regional models.  
159 The GEMS data must be spatially interpolated for the boundaries of each regional model's native  
160 grid and temporally interpolated from the 3-h output interval to the 1-h boundary updates  
161 typically employed by the regional models. Also, the GEMS data contain fairly coarse chemical  
162 speciation of the gaseous organic compounds. Additional disaggregation of these organic  
163 compounds into the specific organic classes used by the tropospheric atmospheric chemistry  
164 mechanisms is usually necessary. In addition, the GEMS aerosol data for sea salt and dust may  
165 need to be redistributed based on the size distribution information carried within the regional  
166 model. Finally, the GEMS data provide information for most of the chemical and aerosol  
167 species needed at the models' boundaries that have significant transport influence. However, all  
168 species are not included in the GEMS data. Modelers may need to provide another source of  
169 boundary concentration data for aerosol sulfate and nitrate, for example, and additional gas-  
170 phase species that may be in their model, unless the boundaries are assumed to be zero, zero-  
171 gradient, or some fixed concentration.

172 There are a few caveats to note with regards to the use of the GEMS data for AQMEII. First,  
173 the SO<sub>2</sub> concentrations were calculated within IFS as a tracer using simple assumptions of  
174 emissions and prescribed loss. No chemical transformations were considered.  
175 Recommendations were made to AQMEII modelers to use the SO<sub>2</sub> data with caution. Sea salt  
176 estimates were made as a function of wind speed and other environmental parameters in the IFS  
177 model. Based on evaluation of the GEMS sea salt data for 2003, quite significant  
178 overpredictions of sea salt aerosol (over 400%) were observed over North America (GEMS,  
179 2010). Preliminary analysis showed this to be true for 2006 as well, so AQMEII modelers were  
180 cautioned on the GEMS sea salt values. Estimates for sea salt over Europe, however, did not  
181 show these same tendencies for overestimation. In addition, organic carbon emissions from fires  
182 in the GEMS data set may have been overestimated in the lower model layers due to the lack of a

183 plume-rise mechanism in the model and an overestimated persistence of the fires from the 8-day  
184 resolution in the data being assimilated into the model. Cautions were therefore extended  
185 regarding the organic carbon data from large fires for AQMEII use.

186

### 187 **3. Other Sources of Boundary Concentrations**

188 The modeling protocol for the AQMEII 2006 model simulations requested that participants  
189 derive their boundary concentrations from the GEMS re-analysis data described above.

190 However, not all participants adhered strictly to this request. In fact, there were a variety of  
191 sources that were accessed for the continental-scale model boundary concentrations. Table 2  
192 presents examples of the various modeling systems used and the source of boundary

193 concentration data in each instance. These data sources include other hemispheric and global  
194 modeling systems, as well as climatological or “background” tropospheric concentrations.

195 Ideally, if all participants had used the same source for the boundary concentration data, as well

196 as a common source for the emissions data, the data analysis and interpretation for the project

197 would be assisted by minimizing confounding effects of different sources of data on model

198 results. Some groups used the requested GEMS data source, as well as alternate sources,

199 providing the data for sensitivity studies on the effect of alternate sources of boundary

200 concentrations on their model simulations.

201

### 202 **4. Impact of Boundary Concentrations on Continental Simulations**

203

204 With typical wind speeds across North America and Europe, inflow air masses can traverse

205 each continent within as few as 3-5 days. Thus the specification of inflow air quality boundary

206 concentrations has the potential for significant impacts on continental model simulations,

207 especially in areas of weaker internal model forcing from source emissions and atmospheric

208 chemistry, and for chemical compounds having lifetimes of this order of magnitude. Pfister et al.

209 (2011) used aircraft and satellite data during the ARCTAS-CARB field campaign during the

210 summer of 2008 to evaluate the MOZART-4 global chemical transport model’s simulation

211 results for its chemical representativeness of chemical inflow to the U.S. west coast. The global

212 model was shown to capture only about half of the observed free tropospheric air pollution

213 variability. Sensitivity simulations with the regional WRF-Chem model, performed as part of

214 the cited work, also showed that the temporal variability in the pollution inflow does clearly  
215 impact modeled surface concentrations over California. It was suggested that time- and space-  
216 varying chemical boundary conditions from global models provide useful input to regional  
217 models, but likely still lead to an underestimate of peak surface concentrations and the variability  
218 associated with long-range transport of air pollution.

219 Hogrefe et al. (2011) performed long-term simulations with the Community Multiscale Air  
220 Quality (CMAQ) model using two sets of chemical boundary conditions, one derived from time-  
221 invariant climatological vertical profiles and the other one from a global chemistry model. The  
222 comparison of both simulations revealed that lateral boundary conditions have a significant  
223 impact on a regional air quality model's ability to simulate long-term O<sub>3</sub> variability and trends,  
224 especially for the middle and lower percentiles of the O<sub>3</sub> distribution. As an illustration, Figure 4  
225 shows time series of May – September average daily maximum 1-h O<sub>3</sub> concentrations derived  
226 from observations and these two sets of CMAQ simulations for the time period from 1988 to  
227 2005. It can be seen that the choice of boundary conditions affects the magnitude of the mean  
228 concentrations as well as their inter-annual variability and trends. In this particular example, the  
229 CMAQ simulation using the time-invariant boundary conditions shows better agreement with the  
230 observations in terms of absolute concentrations and trends while the CMAQ simulation using  
231 boundary conditions derived from the global model shows better agreement in terms of inter-  
232 annual variability.

233 Li et al. (2002) used a five-year (1993-1997) simulation with the GEOS-Chem CTM and  
234 showed that North American pollution enhances surface O<sub>3</sub> in continental Europe by 2–4 ppbv  
235 on average in summer and by 5–10 ppbv during transatlantic transport events. Specifying the  
236 model continental-scale O<sub>3</sub> boundary concentrations correctly is significant in that the North  
237 American influence on surface O<sub>3</sub> in Europe is particularly strong at the thresholds used for the  
238 European air quality standards (55–65 ppbv). Simulating the daily variability of O<sub>3</sub> boundary  
239 concentrations was also shown to significantly improve both variability and biases of simulated  
240 daily O<sub>3</sub> maxima in Europe, in particular for the most frequent non-extreme values (Szopa et al.,  
241 2009).

242 Ratigejev et al. (2010) demonstrate that global CTMs have difficulty reproducing synoptic-  
243 scale pollution plumes during long-range transport. Numerical diffusion interacting with non-  
244 uniform atmospheric flows dissipates the plumes faster than ambient observations suggest. The

245 authors state that novel numerical methods, such as adaptive grids or embedded Lagrangian  
246 plumes, may circumvent the problem of accurately sustaining the plume integrity. Makar et al.  
247 (2010) evaluated ten different approaches for applying lateral and top climatological boundary  
248 concentrations for O<sub>3</sub> using the AURAMS regional CTM. They found that dynamic adjustments  
249 to the O<sub>3</sub> profile in response to the model-estimated tropopause height were needed to better  
250 match mass consistency between chemical and meteorological models. Their results highlight  
251 the importance of evaluating boundary concentrations and mass consistency/correction  
252 algorithms with three-dimensional measurements.

253

#### 254 *4.1 CMAQ Model – North America application*

255 The U.S. EPA contributed results to AQMEII from a 2006 North American simulation from  
256 their CMAQ model. The model domain included all of the continental U.S. (except Alaska),  
257 southern Canada, and northern Mexico. Meteorological data for the CMAQ simulation were  
258 derived from a continental model run of the Weather Research and Forecasting (WRF) model  
259 using four-dimensional data assimilation. The CMAQ model also made use of the standard  
260 protocol data provided by AQMEII for emissions and boundary concentrations (GEMS dataset).  
261 To assess the adequacy of the GEMS data for providing inflow O<sub>3</sub> boundary concentrations, we  
262 have examined the performance of the CMAQ model using observed data from the INTEX-B  
263 Ozonesonde Network Study (IONS) of 2006 (Tarasick et al., 2010) for sounding locations near  
264 the west (inflow) coast of North America. The IONS 2006 study provided a total of 740  
265 ozonesonde profiles from 23 sites across North America. Figure 5 illustrates the locations of  
266 these sites within the CMAQ modeling domain, with the shaded area indicating the region of  
267 interest for examining the boundary concentration impacts.

268 Figures 6a and 6b present the results of the CMAQ simulation and the observed O<sub>3</sub> vertical  
269 profile from the Trinidad Head site on the northern California coast averaged over all March  
270 (n=6) and August (n=30) profiles, respectively. For both months, the model and observed  
271 profiles agree fairly well at altitudes corresponding to the upper troposphere and stratosphere.  
272 Here, the model is greatly influenced by the boundary concentrations as there are no local  
273 emissions and little atmospheric chemistry to influence the estimated concentrations. However,  
274 in the lower and mid troposphere, the model significantly underestimates the O<sub>3</sub> concentrations  
275 compared to the observed profile. Also indicated on the figures are the concentrations from

276 CMAQ attributable to a boundary concentration tracer for O<sub>3</sub>. In these calculations, the impact  
277 of the spatially and temporally varying O<sub>3</sub> boundary conditions was tracked using a tracer  
278 species that underwent advective, turbulent, and cloud transport, and wet and dry deposition  
279 similar to O<sub>3</sub>. Since the tracer was not subject to any chemical loss, its inferred impact on the net  
280 simulated O<sub>3</sub> may be slightly overestimated. Nevertheless, the tracer provides a direct estimate  
281 of the impact of the GEMS boundary concentrations on simulated O<sub>3</sub> distributions and trends.  
282 With little local photochemistry occurring in March, it is evident that the lower portion of the  
283 profile is completely controlled by the boundary concentrations, while in August with more  
284 active photochemistry the lowest portion of the profile shows enhanced concentrations as  
285 compared to the boundary tracer. This is further illustrated in Figure 7 which presents the  
286 average fractional contribution of the boundary conditions to the simulated vertical profile at  
287 Trinidad Head for the months of March and August 2006. It is evident that above 3-4 km the  
288 simulated O<sub>3</sub> variability is largely dictated by the boundary condition specification.

289 Similar analyses for the Kelowna site in British Columbia, Canada are presented in Figure 8.  
290 (There were 2 profiles available in March and 26 in August at Kelowna.) Results of these  
291 comparisons are comparable to those of the Trinidad Head site, although this site shows larger  
292 deviations in the upper portion of the profiles between CMAQ and the observed data. Results of  
293 comparisons at other west coast sites (not shown) demonstrate similar behavior, with CMAQ  
294 generally underestimating O<sub>3</sub> near the surface and in the lower and mid troposphere, with the  
295 greatest discrepancies in winter and the least in summer. From these profiles it appears that the  
296 O<sub>3</sub> boundary concentration tracer, as a surrogate for the GEMS data, has considerably  
297 underestimated the inflow O<sub>3</sub> to the west coast of North America in the lower troposphere,  
298 especially during the winter and spring. It is not surprising that the GEMS data should better  
299 reflect the observed O<sub>3</sub> profile in the upper levels as compared to levels closer to the surface.  
300 The GEMS re-analyses have made extensive use of data assimilation for O<sub>3</sub> based on satellite  
301 retrievals. These derived measurements are most accurate for the stratospheric O<sub>3</sub> burden and  
302 become more uncertain in the lower portions of the profile. In the lower levels, the GEMS data  
303 are more reflective of the results of the MOZART-3 model simulations which appear to have  
304 systematically underestimated tropospheric O<sub>3</sub> in the northeast Pacific region, and generated a  
305 low bias in the specified inflow concentrations for North America, possibly due to emissions  
306 uncertainties and an overestimation of dry deposition.

307 A distinct advantage of the data assimilation aspect of the GEMS re-analysis is that real-time  
308 events, such as large forest fires or dust storms, are seen by satellite sensors and can be  
309 incorporated in the model simulation. Figure 9 shows the vertical profiles of primary organic  
310 particulate matter (OM) along each boundary of the CMAQ North American domain averaged  
311 over the period of 21-30 June 2006 from the GEMS database. One can readily see the strong  
312 impact of a large wildfire occurring at the time in the Canadian boreal forest. The impact on  
313 surface layer CMAQ estimates of primary organic particulate matter is seen in Figure 10 in  
314 which the 01 UTC concentrations are presented for 30 June 2006. The effects of the wildfires  
315 north of the CMAQ domain are evident as the boundary concentrations have been advected into  
316 the northern portion of CMAQ's computational domain. Satellite measurements confirm the  
317 elevated aerosol loadings in this area from the wildfires.

318

#### 319 *4.2 CHIMERE Model – North America application*

320 The sensitivity of concentrations simulated by a regional model to chemical boundary  
321 conditions was tested by IPSL-France using the CHIMERE model (Bessagnet et al., 2004), by  
322 using in separate simulations the GEMS boundary conditions provided to AQMEII (Simulation  
323 A) and the boundary conditions typically used in CHIMERE studies, as provided by monthly  
324 climatologies of the LMDzINCA global model (Hauglustaine et al., 2004) for gas-phase species  
325 and the GOCART model for aerosol species (Ginoux et al., 2001). For this simulation (B),  
326 carried out in exactly the same setting as for Simulation A for other model parameters, boundary  
327 conditions are constant within each month but vary along model boundaries. It must be noted  
328 that CHIMERE only simulates concentrations within the lower atmosphere: it has a top boundary  
329 at 500 hPa. Concentrations within the modeling domain are thus sensitive to both lateral and top  
330 boundary concentrations.

331 The mean O<sub>3</sub> surface concentration differences between Simulations B and A have been  
332 calculated for each season (Winter=DJF, Spring=MAM, Summer=JJA, Fall=SON) and are  
333 represented in Figure 11. The sensitivity to O<sub>3</sub> boundary concentrations differs from one season  
334 to another. In winter and spring, strong winds and vertical mixing induce a larger sensitivity to  
335 boundary concentrations than in summer and fall. For instance, in winter, seasonal mean  
336 concentration differences between the two simulations in the center of the domain and those near  
337 the boundaries vary by a factor of two or so. In contrast, in summer and fall the concentration

338 differences vary by more than a factor of 5 between the center of the domain and the regions near  
339 the boundaries, indicating that boundary conditions have a relatively smaller impact on the inner  
340 portions of the domain compared to winter and spring. However, in all seasons studied, the  
341 impact of boundary conditions extends inland far from the boundaries. The Central-East U.S.  
342 shows the smallest influence from the boundary conditions.

343 Note also that the difference between mean LMDzINCA-driven and MOZART-driven  
344 simulations remains positive across the domain, because the LMDzINCA O<sub>3</sub> boundary  
345 conditions are higher than the MOZART ones. This difference is largest in the winter season,  
346 and reaches about 15 ppb, while in summer it reaches 10 ppb. The magnitude of these  
347 differences in seasonal mean concentrations caused by different boundary conditions is  
348 comparable to those shown in Hogrefe et al. (2011; see figure 11 therein).

349

#### 350 *4.3 CHIMERE Model – Europe application*

351 The CHIMERE model has also been applied over Europe using the TNO emissions inventory  
352 at a 0.25° horizontal resolution by INERIS-France. As in the North American case, the model  
353 domain extends vertically to 500hPa. To assess the impact of the temporal resolution of the  
354 boundary concentrations (BCs) on air quality modeled in the regional domain, the whole year  
355 2006 has been run twice with 3-hourly GEMS BCs for both gaseous species and aerosols (3HR),  
356 and with a monthly climatology derived from the same dataset (gas and aerosols as well; CST).  
357 In the CST run, for a given time in a month, the model is driven with constant BCs; no  
358 interpolation is performed between two consecutive months.

359 In Figure 12 we display the average difference between the simulations with 3-hourly BCs and  
360 the monthly climatology for O<sub>3</sub>. With both sets of BCs derived from the same global  
361 simulations, these plots would exhibit a null geographical variability if the regional model  
362 behaved as a linear operator. Since that is obviously not the case, these plots reflect the  
363 combined impact of (1) the non-linearity of the regional model together with (2) the skewness of  
364 the O<sub>3</sub> distribution at the boundaries. For instance, the difference is consistently negative at the  
365 southern boundary showing that the mean BCs (used in the CST run) lead to an overestimation  
366 of O<sub>3</sub> compared to the 3HR BCs. On the western and northern parts of the domain, the situation  
367 is less straightforward. In summer (JJA), climatological BCs lead to an overestimation of O<sub>3</sub>, but  
368 in spring and fall they yield an underestimation compared to time-varying fields. It is likely that

369 stratospheric intrusions into the troposphere captured in the GEMS re-analysis (which may have  
370 an impact in the CHIMERE model down to the surface by means of vertical mixing) play an  
371 important role on these patterns. As isolated, yet very concentrated, layers of O<sub>3</sub>, these events  
372 have a larger impact on the average than on the median concentrations. Depending on their  
373 geographical and seasonal variability they could thus be responsible for the patterns observed in  
374 Figure 12.

375 Figure 13 shows the difference of standard deviation between the 3HR and CST simulation  
376 results for both O<sub>3</sub> and PM10 concentrations. Using the 3HR fields at the boundary has a  
377 noticeable impact on the outskirts of the model domain. Since Europe is mainly affected by  
378 sporadic and large dust outbreaks from the Sahara, the southern boundary displays higher  
379 variability with 3HR BCs. The eastern part of the domain includes a fire emission zone in  
380 Russia, which leads to higher standard deviations in this region. Since sea salt BCs have been  
381 removed in the GEMS dataset there are no specific patterns observed in the western and northern  
382 parts of the domain. Table 3 shows the global standard deviation of daily mean concentrations  
383 of O<sub>3</sub>, NO<sub>2</sub>, and PM10 for all European air quality monitoring stations taken from the AIRBASE  
384 dataset (all available stations). For short-lived species like NO<sub>2</sub>, the time-varying BCs have a  
385 negligible impact. However, for both O<sub>3</sub> and PM10, using the 3HR fields at the boundaries  
386 contributes to obtaining a slightly larger variability that is more in agreement with the  
387 observations for O<sub>3</sub> and NO<sub>2</sub>. The time variability is impaired for PM10 showing that the  
388 predictability of dust events (intensity and occurrence) remains difficult as shown by Menut et al.  
389 (2009). If dust models can provide a better measure of variability on seasonal or monthly bases,  
390 these models could better predict dust concentrations over Europe on a daily basis. It should be  
391 noted that the estimates provided by this comparison at the station locations overly weight the  
392 center of the domain, where stations are by far more numerous and the impact of BCs less  
393 noticeable.

394 Recently Pfister et al. (2011) conducted similar sensitivity experiments with the WRF-Chem  
395 model in which boundary concentrations for North American inflow were derived from the  
396 MOZART-4 global chemical transport model using 3-hourly varying data as well as an  
397 experiment using boundary data averaged over their simulation period (14-30 June 2008; during  
398 ARCTAS-CARB field experiments). Their results focused on inflow to California during that  
399 period, and much like the results presented here, the variability in boundary concentrations was

400 better captured with the higher temporal resolution. One difference that was noted was in the  
401 mean O<sub>3</sub> concentrations at the boundaries, where Pfister et al. (2011) reported the same mean O<sub>3</sub>  
402 values irrespective of the temporal averaging at the boundaries, while the current study noted  
403 differences in the means based on the temporal averaging. This discrepancy in the findings is  
404 likely due to the longer simulation period used here (one year) compared to the 17-day  
405 simulation period in the Pfister study. The longer simulation allowed for additional anomalous  
406 events, such as stratospheric intrusions of O<sub>3</sub> into the lower troposphere, to affect the average in  
407 non-linear fashion.

408

#### 409 *4.4 CMAQ Model – Europe application*

410 The CMAQ model was applied over the European domain for the year 2006 using the input  
411 datasets prescribed for AQMEII (including the GEMS boundary concentrations) by the  
412 University of Hertfordshire-UK. An evaluation of the CMAQ calculations, for the continental-  
413 scale domains in North America and Europe, is given in Appel et al. (2011; this issue). To  
414 examine the impacts of the boundary concentrations on the model results, an additional  
415 simulation was performed for 2006 using boundary concentrations provided by the global  
416 chemical transport model GEOS-Chem, version 8-03-01 (see [http://wiki.seas.harvard.edu/geos-  
417 chem/index.php/Main\\_Page](http://wiki.seas.harvard.edu/geos-chem/index.php/Main_Page)). The GEOS-Chem model was run at a 2° x 2.5° horizontal  
418 resolution with 47 hybrid pressure-sigma vertical levels. The model was driven by assimilated  
419 meteorological data from the Goddard Earth Observing System (GEOS-5) at the NASA Global  
420 Modeling and Assimilation Office (GMAO). We used the chemistry mechanism NO<sub>x</sub>-O<sub>x</sub>-  
421 hydrocarbon-aerosol to simulate O<sub>3</sub> and aerosols (Jacob, 2000; Bey et al., 2001). The aerosol  
422 components included sulfate, nitrate, ammonium, black carbon, organics, mineral dust, and sea  
423 salt (see Park et al., 2004; Hu et al., 2007). The emission inventories were separated into four  
424 source categories: anthropogenic, biomass, biofuel, and biogenic. Sources of mineral dust and  
425 sea salt are dealt with separately. The anthropogenic emissions were obtained from the Global  
426 Emissions Inventory Activity (GEIA) dataset. Biomass burning and biofuel-use emissions were  
427 derived from Duncan et al. (2007). Biogenic emissions included isoprene, methyl butenol,  
428 acetone, and alkene.

429 As in Section 4.1, we focus on the adequacy of the boundary concentrations data for setting  
430 the inflow of O<sub>3</sub> into the modeling domain. Figure 14 presents the observed and modeled

431 vertical distributions of O<sub>3</sub> at Lerwick, Shetland Mainland, UK, for the year 2006. The Lerwick  
432 Observatory is situated in a remote location representative of background (inflow) atmospheric  
433 concentrations. The time-height evolution of O<sub>3</sub> in Figure 14a was compiled from measurements  
434 by a UK Met Office ozonesonde of the Electrochemical Concentration Cell (ECC) type (Komhyr  
435 et al., 1995). The two model calculations agree fairly well with the observations at altitudes  
436 above 6-8 km (i.e., in the upper troposphere/lower stratosphere). While the GEMS re-analysis  
437 included the assimilation of O<sub>3</sub> data from satellite observations, the GEOS-Chem simulation  
438 included stratospheric O<sub>3</sub> chemistry based on a climatological representation of species sources  
439 and sinks. Both techniques appeared to work well in reproducing the O<sub>3</sub> profile at the higher  
440 altitudes. Interestingly, the agreement degrades in the lower troposphere when using the GEMS  
441 boundary concentrations, while it remains fair when using those provided by GEOS-Chem. The  
442 difference between the observed O<sub>3</sub> concentrations and those of the simulation using the GEMS  
443 boundary concentrations is most dramatic for the first four months of 2006, with low biases as  
444 large as 20 ppb.

445 Similar findings can be observed in Figure 15, where the observed and modeled ground-level  
446 O<sub>3</sub> concentrations at Mace Head, Republic of Ireland, are shown. The location of the monitoring  
447 station on the Atlantic Coast makes it a representative site for background concentrations of  
448 substances in the atmosphere. The O<sub>3</sub> concentration at the site, simulated using the GEMS  
449 boundary concentrations, appears to be biased low for the first four months of 2006. Afterwards,  
450 the two model calculations give comparable results. This highlights the importance of boundary  
451 concentrations in setting the baseline concentrations in the modeling domain.

452

## 453 **5.0 Summary and Conclusions**

454

455 The AQMEII project on regional-scale air quality model system evaluation and inter-  
456 comparison has proposed the use of a common set of boundary concentrations to be specified to  
457 the regional modelers for all to use in an effort to minimize differences across the models from  
458 this particular aspect of the modeling protocol. The GEMS re-analysis air quality dataset has  
459 been provided for this purpose from the ECMWF for the AQMEII focus year of 2006. The re-  
460 analysis is produced by assimilating satellite observations of select chemical and aerosol species  
461 into a coupled model system, which consists of ECMWF's IFS and the MOZART-3 CTM. The

462 resulting dataset provides spatially- and temporally-resolved information on concentrations of  
463 most of the key transported species of interest to the AQMEII regional modelers for use in their  
464 modeling systems. Each regional modeling group then must cast these data into forms directly  
465 usable by their particular model. This processing may include further spatial and temporal  
466 interpolations as well as chemical speciation of the trace gases and aerosols for the particular  
467 chemical and aerosol mechanisms used by the model.

468 In this study we found that specification of O<sub>3</sub> profiles from the GEMS dataset at the  
469 boundaries of the North American and European modeling domains for the 2006 simulations  
470 offered good agreement in the upper troposphere and lower stratosphere with an independent set  
471 of observations from ozonesondes. For the North American domain, the O<sub>3</sub> boundary  
472 concentrations throughout 2006 were underestimated in the GEMS dataset in the lower to mid  
473 troposphere, with greater biases in winter and spring and lower biases in summer. In the  
474 European simulations the GEMS dataset yielded O<sub>3</sub> boundary concentrations that were  
475 consistent with ozonesonde observations except for the first quarter of 2006 when the lower  
476 tropospheric O<sub>3</sub> values were biased low by as much as 20 ppb. SO<sub>2</sub> concentrations in the GEMS  
477 dataset were derived from simple assumptions and not based on a complete chemical description  
478 in the global modeling. AQMEII modelers were cautioned regarding their use for continental  
479 boundary concentrations. For particulate matter we found that organic carbon from large fires  
480 was well detected by the GEMS data assimilation system, but that concentrations could be  
481 overestimated near the surface due to lack of a plume rise mechanism and eight-day temporal  
482 averaging of fire emissions. Sea salt was greatly overestimated near the boundaries of the North  
483 American domain, although the bias was less over the North Atlantic near the borders of the  
484 European domain. The GEMS dataset did not provide estimates of particulate sulfate or nitrate.

485 Specification of boundary concentrations is a required element in modeling with limited-area  
486 air quality models, such as regional- to continental-scale CTMs. The limited area models are  
487 typically quite sensitive to these specified concentrations, especially in areas of limited internal  
488 forcing by emissions and chemistry within the model's computational domain. Sensitivity  
489 simulations performed with the CHIMERE model emphasize that the impact of O<sub>3</sub> boundary  
490 concentrations can extend far into the model domain beyond the boundaries. These studies also  
491 show that boundary concentrations derived from monthly O<sub>3</sub> climatologies can deviate  
492 substantially from more temporally-resolved concentrations. The tropospheric impacts of

493 stratospheric O<sub>3</sub> intrusion events, for example, can be greatly damped or eliminated by monthly  
494 averages.

495 Long-duration simulations, such as the full-year simulations performed within the AQMEII  
496 project, require boundary concentrations that reflect not only day-to-day variations but also  
497 seasonal and inter-annual changes in the global environment. Use of global CTMs to provide  
498 these boundary concentrations is a logical and convenient mechanism for their specification. It  
499 should be noted, however, as seen in these AQMEII model results, as well as the results  
500 presented in Hogrefe et al. (2011), that the global models may contain errors or biases in their  
501 simulated results that can then propagate into the regional models through the boundaries and  
502 affect the results within the model domain. The use of data assimilation in the global models can  
503 help minimize these errors, but cannot eradicate them. The assimilated satellite observations  
504 provide mainly vertically integrated column values, which makes it more difficult for the  
505 assimilating model to obtain realistic concentration profiles close to the surface. Examining  
506 several sources of boundary concentrations, such as alternate global CTMs, may provide useful  
507 information to modelers on ranges of boundary concentrations to consider. With the tightening  
508 of air quality standards and the imposition of emissions control programs, air pollution levels  
509 have generally been declining in many nations, leading to the need to better quantify background  
510 pollution as an “irreducible” portion of the local pollutant burden. Therefore the process of  
511 specifying boundary concentrations for limited area models is an important issue and must be  
512 performed with careful scrutiny to assure the best possible outcome from regional-scale model  
513 simulations.

514

## 515 **Acknowledgements**

516

517 In addition to the data sources and organizations acknowledged in the Foreword to this  
518 AQMEII Special Issue, we would like to note that the Mace Head O<sub>3</sub> data were obtained from  
519 the Defra UK Air Information Resource (UK AIR, <http://uk-air.defra.gov.uk>). Participation in  
520 this AQMEII study by IPSL and INERIS was supported by the Institut National des Sciences de  
521 l’Univers in France through the AQMEII.fr project, and the SALUT’AIR program funded by  
522 PRIMEQUAL. A special note of appreciation is extended to the staff and collaborators in the  
523 GEMS project within the European Centre for Medium-Range Weather Forecasting (ECMWF)

524 and other participating organizations for making possible the use of GEMS air quality re-analysis  
525 data in the AQMEII project, and for helping process and explain the data details. Thanks are  
526 extended to Angela Benedetti, Johannes Kaiser, Jean-Jacques Morcrette, and Adrian Simmons  
527 (ECMWF); Martin Schultz (FZ-Jülich); Vincent-Henri Peuch (Meteo-France); Darius Ceburnis  
528 (National University of Ireland); and Chris Nolte (U.S. EPA).

529       The views expressed here are those of the authors and do not necessarily reflect the views  
530 and policies of the U.S. Environmental Protection Agency or any other organization participating  
531 in the AQMEII project. This manuscript has been subjected to U.S. EPA review and approved  
532 for publication.

533

534 **References**

535

536 Appel K.W., C. Chemel, S.J. Roselle, X.V. Francis, T. Pierce, S.T. Rao, R.S. Sokhi, and S.  
537 Galmarini, 2011. Examination of the Community Multiscale Air Quality (CMAQ) model  
538 performance for North America and Europe for the AQMEII project. submitted to  
539 Atmospheric Environment (this issue).

540 Benedetti, A., J.-J. Morcrette, O. Boucher, et al., 2009. Aerosol analysis and forecast in the  
541 European Centre for Medium-Range Weather Forecasts Integrated Forecast System: 2. Data  
542 assimilation. Journal of Geophysical Research, 114, D13205, doi:10.1029/2008JD011115.

543 Bessagnet, B., A. Hodzic, R. Vautard, M. Beekmann, S. Cheinet, C. Honoré, C. Liousse and L.  
544 Rouil, 2004. Aerosol modeling with CHIMERE: preliminary evaluation at the continental  
545 scale. Atmospheric Environment, 38, 2803-2817.

546 Bey I., D.J. Jacob, R.M. Yantosca, J.A. Logan, B. Field, A.M. Fiore, Q. Li, H. Liu, L.J. Mickley,  
547 and M. Schultz, 2001. Global modeling of tropospheric chemistry with assimilated  
548 meteorology: Model description and evaluation. Journal of Geophysical Research, 106,  
549 23,073-23,096.

550 Bond, T.C., D.G. Streets, K.F. Yarber, S.M. Nelson, J.-H. Woo, and Z. Klimont, 2004. A  
551 technology-based global inventory of black and organic carbon emissions from combustion.  
552 Journal of Geophysical Research, 109, D14203, doi:10.1029/2003JD003697.

553 Bousserez, N., J.-L. Atti'e, V.-H. Peuch, M. Michou, and G. Pfister, 2007. Evaluation of the  
554 MOCAGE chemistry and transport model during the ICARTT/ITOP experiment. Journal of  
555 Geophysical Research, 112, D10S42, doi:10.1029/2006JD007595.

556 Dennis, R., T. Fox, M. Fuentes, A. Gilliland, S. Hanna, C. Hogrefe, J. Irwin, S.T. Rao, R.  
557 Scheffe, K. Schere, D. Steyn, and A. Venkatram, 2010. A framework for evaluating regional-  
558 scale numerical photochemical modeling systems. Environmental Fluid Mechanics, 10, 471-  
559 489.

560 Duncan, B.N., J.A. Logan, I. Bey, I.A. Megretskaia, R.M. Yantosca, P.C. Novelli, N.B. Jones,  
561 and C.P. Rinsland, 2007. The global budget of CO, 1988-1997: source estimates and  
562 validation with a global model. Journal of Geophysical Research, 112, D22301,  
563 doi:10.1029/2007JD008459.

564 Eder, B., D. Kang, S.T. Rao, R. Mathur, S. Yu, T. Otte, K. Schere, R. Wayland, S. Jackson, P.  
565 Davidson, J. McQueen, and G. Bridgers, 2010. Using national air quality forecast guidance  
566 to develop local air quality index forecasts. *Bulletin of the American Meteorological Society*,  
567 91, 313-326.

568 Flemming, J., A. Inness, H. Flentje, V. Huijnen, P. Moinat, M.G. Schultz, and O. Stein, 2009.  
569 Coupling global chemistry transport models to ECMWF's integrated forecast system.  
570 *Geoscientific Model Development*, 2, 253-265.

571 Flemming, J., A. Inness, L. Jones, H.J. Eskes, V. Huijnen, M.G. Schultz, O. Stein, D. Cariolle,  
572 D. Kinnison, and G. Brasseur, 2011. Forecasts and assimilation experiments of the Antarctic  
573 ozone hole 2008. *Atmospheric Chemistry and Physics*, 11, 1961-1977, doi:10.5194/acp-11-  
574 1961-2011.

575 GEMS, 2010. A Monitoring and Forecasting System for Atmospheric Composition. Final report  
576 of the GEMS project. Available from <http://www.gmes-atmosphere.eu/documents/reports/>.  
577 184pp.

578 Ginoux, P., M. Chin, I. Tegen, J.M. Prospero, B. Holben, O. Dubovik, and S.-J. Lin, 2001.  
579 Sources and distributions of dust aerosols simulated with the GOCART model. *Journal of*  
580 *Geophysical Research*, 106, 20255-20273.

581 Hauglustaine, D.A., F. Hourdin, L. Jourdain, M.A. Filiberti, S. Walters, J.F. Lamarque, and E.A.  
582 Holland, 2004. Interactive chemistry in the Laboratoire de Météorologie Dynamique general  
583 circulation model: Description and background tropospheric chemistry evaluation, *Journal of*  
584 *Geophysical Research*, 109, D04314, doi :10.1029/2003JD003957.

585 Hogrefe, C., W. Hao, E.E. Zalewsky, J.-Y. Ku, B. Lynn, C. Rosenzweig, M.G. Schultz, S. Rast,  
586 M.J. Newchurch, L. Wang, P.L. Kinney, and G. Sistla, 2011. An analysis of long-term  
587 regional-scale ozone simulations over the Northeastern United States: variability and trends.  
588 *Atmospheric Chemistry and Physics*, 11, 567-582, doi:10.5194/acp-11-567-2011.

589 Hollingsworth, A., R.J. Engelen, A. Benedetti, A. Dethof, J. Flemming, J.W. Kaiser, J.-J.  
590 Morcrette, A.J. Simmons, C. Textor, O. Boucher, F. Chevallier, P. Rayner, H. Elbern, H.  
591 Eskes, C. Granier, V.-H. Peuch, L. Rouil, M.G. Schultz, 2008. Toward a monitoring and  
592 forecasting system for atmospheric composition: The GEMS Project. *Bulletin of the*  
593 *American Meteorological Society*, 89, 1147-1164.

594 Honoré, C., L. Rouïl, R. Vautard, M. Beekmann, B. Bessagnet, A. Dufour, C. Elichegaray, J.-M.  
595 Flaud, L. Malherbe, F. Meleux, L. Menut, D. Martin, A. Peuch, V.-H. Peuch, and N. Poisson,  
596 2009. PREV'AIR: an operational forecasting and mapping system for air quality in Europe.  
597 *Bulletin of the American Meteorological Society*, 90, 73-83.

598 Hu, R.-M., R.V. Martin, and T.D. Fairlie, 2007. Global retrieval of columnar aerosol single  
599 scattering albedo from space-based observations, *Journal of Geophysical Research*, 112,  
600 D02204, doi:10.1029/2005JD006832.

601 Huijnen, V., J. Williams, M. van Weele, T. van Noije, M. Krol, F. Dentener, A. Segers, S.  
602 Houweling, et al., 2010. The global chemistry transport model TM5: description and  
603 evaluation of the tropospheric chemistry version 3.0. *Geoscientific Model Development*, 3,  
604 445-473, doi:10.5194/gmd-3-445-2010.

605 Inness, A., J. Flemming, M. Suttie and L. Jones, 2009. GEMS data assimilation system for  
606 chemically reactive gases. Technical Memorandum No. 587, European Centre for Medium-  
607 Range Weather Forecasts (ECMWF), Reading, UK.

608 Jacob, D.J., 2000. Heterogeneous chemistry and tropospheric ozone. *Atmospheric Environment*,  
609 34, 2131-2159.

610 Kinnison, D.E., G.P. Brasseur, S. Walters, R.R. Garcia, D.R. Marsh, F. Sassi, V.L. Harvey, C.E.  
611 Randall, L. Emmons, J.F. Lamarque, P. Hess, J.J. Orlando, X. Tie, W. Randel, L.L. Pan, A.  
612 Gettelman, C. Granier, T. Diehl, U. Niemeier, and A.J. Simmons, 2007. Sensitivity of  
613 chemical tracers to meteorological parameters in the MOZART-3 chemical transport model.  
614 *Journal of Geophysical Research*, 112, D03303, doi:10.1029/2008JD010739.

615 Komhyr, W.D., R.A. Barnes, G.B. Brothers, J.A. Lathrop, and D.P. Opperman, 1995.  
616 Electrochemical Concentration Cell ozonesonde performance evaluation during STOIC  
617 1989. *Journal of Geophysical Research*, 100, 9231-9244.

618 Li, Q., D.J. Jacob, P.I. Palmer, B.N. Duncan, B.D. Field, A.M. Fiore, R.M. Yantosca, D. Parrish,  
619 P.G. Simmonds, and S. Oltzman, 2002. Transatlantic transport of pollution and its effects on  
620 surface ozone in Europe and North America. *Journal of Geophysical Research*, 107(D13),  
621 4166, doi:10.1029/2001JD001422.

622 Makar, P.A., W. Gong, C. Mooney, J. Zhang, D. Davignon, M. Samaali, M.D. Moran, H.  
623 He, D.W. Tarasick, D. Sills, and J. Chen, 2010. Dynamic adjustment of climatological ozone

624 boundary conditions for air-quality forecasts. *Atmospheric Chemistry and Physics*, 10, 8997-  
625 9015.

626 McKeen, S., J. Wilczak, G. Grell, I. Djalalova, S. Peckham, E.-Y. Hsie, W. Gong, V. Bouchet, S.  
627 Menard, R. Moffet, J. McHenry, J. McQueen, Y. Tang, G. Carmichael, M. Pagowski, A.  
628 Chan, T. Dye, G. Frost, P. Lee, and R. Mathur, 2005. Assessment of an ensemble of seven  
629 real-time ozone forecasts over eastern North America during the summer of 2004. *Journal of*  
630 *Geophysical Research*, 110, D21307, doi:10.1029/2005JD005858.

631 Menut L., I. Chiapello and C. Moulin, 2009. Previsibility of mineral dust concentrations: The  
632 CHIMERE-DUST forecast during the first AMMA experiment dry season. *Journal of*  
633 *Geophysical Research*, 114, D07202, doi:10.1029/2008JD010523.

634 Morcrette, J.-J., O. Boucher, L. Jones, D. Salmond, P. Bechtold, A. Beljaars, A. Benedetti, A.  
635 Bonet, J. W. Kaiser, M. Razinger, M. Schulz, S. Serrar, A. J. Simmons, M. Sofiev, M. Suttie,  
636 A. M. Tompkins, and A. Untch, 2009. Aerosol analysis and forecast in the ECMWF  
637 Integrated Forecast System. Part I: Forward modeling. *Journal of Geophysical Research*,  
638 114D, D06206, doi:10.1029/2008JD011235.

639 Park, R.J., D.J. Jacob, B.D. Field, R.M. Yantosca, and M. Chin, 2004. Natural and transboundary  
640 pollution influences on sulfate-nitrate-ammonium aerosols in the United States: implications  
641 for policy. *Journal of Geophysical Research*, 109, D15204, doi:10.1029/2003JD004473.

642 Pfister, G.G., D. Parrish, H. Worden, L.K. Emmons, D.P. Edwards, C. Wiedinmyer, G.S. Diskin,  
643 G. Huey, S.J. Oltmans, V. Thouret, A. Weinheimer, and A. Wisthaler, 2011. Characterizing  
644 summertime chemical boundary conditions for airmasses entering the U.S. West Coast.  
645 *Atmospheric Chemistry and Physics*, 11, 1769-1790.

646 Rabier, F., H. Järvinen, E. Klinker, J.F. Mahfouf, and A.J. Simmons, 2000. The ECMWF  
647 operational implementation of four dimensional variational assimilation. Part 1:  
648 Experimental results with simplified physics. *Quarterly Journal of the Royal Meteorological*  
649 *Society*, 126, 1143-1170.

650 Rao, S.T., S. Galmarini, and K. Puckett, 2011. Air Quality Model Evaluation International  
651 Initiative (AQMEII): Advancing state-of-science in regional photochemical modeling and its  
652 applications. *Bulletin of the American Meteorological Society*, 92, 23-30.

653 Rastigejev, Y., R. Park, M.P. Brenner, and D.J. Jacob, 2010. Resolving intercontinental pollution  
654 plumes in global models of atmospheric transport. *Journal of Geophysical Research*, 115,  
655 D02302, doi:10.1029/2009JD012568, 2010

656 Schultz, M.G., T. Pulles, R. Brand, M. van het Bolscher, and S.B. Dalsøren, 2009. A global data  
657 set of anthropogenic CO, NO<sub>x</sub>, and NMVOC emissions for 1960–2000. Available at:  
658 <http://retro.enes.org/data/emissions.shtml>.

659 Szopa, S., G. Forêt, L. Menut, and A. Cozic, 2009. Impact of large-scale circulation on European  
660 summer surface ozone and consequences for modeling forecast. *Atmospheric Environment*,  
661 43, 1189-1195.

662 Tarasick, D.W., et al., 2010. High-resolution tropospheric ozone fields for INTEX and ARCTAS  
663 from IONS ozonesondes. *Journal of Geophysical Research*, 115, D20301,  
664 doi:10.1029/2009JD012918.

665 van der Werf, G.R., J.T. Randerson, L. Giglio, G.J. Collatz, P.S. Kasibhatla, and A.F. Arellano  
666 Jr., 2006. Interannual variability in global biomass burning emissions from 1997 to 2004.  
667 *Atmospheric Chemistry and Physics*, 6, 3423–3441.

668 Vautard, R., P. Builtjes, P. Thunis, C. Cuvelier, M. Bedogni, B. Bessagnet, C. Honore, N.  
669 Moussiopoulos, G. Pirovano, M. Schaap, R. Stern, L. Tarrason, and P. Wind, 2007.  
670 Evaluation and inter-comparison of ozone and PM<sub>10</sub> simulations by several chemistry  
671 transport models over four European cities within the CityDelta project. *Atmospheric*  
672 *Environment*, 41, 173-188.

673

674 Table 1. Gas-phase reactive chemical and aerosol species extracted from GEMS data  
 675

<b>Gas-phase Reactive Chemical Species<sup>1</sup></b>		
O <sub>3</sub> (ozone)	HNO <sub>3</sub> (nitric acid)	C <sub>2</sub> H <sub>6</sub> (ethane)
CO (carbon monoxide)	HO <sub>2</sub> NO <sub>2</sub> (peroxynitric acid)	ISOP (isoprene)
CH <sub>2</sub> O (formaldehyde)	PAN (peroxy acetyl nitrate)	TOLUENE (sum of C <sub>7</sub> ,C <sub>8</sub> ,C <sub>9</sub> aromatics)
NO (nitrogen oxide)	CH <sub>4</sub> (methane)	BIGENE (>C <sub>3</sub> alkenes)
NO <sub>2</sub> (nitrogen dioxide)	CH <sub>3</sub> CHO (acetaldehyde)	BIGALK (>C <sub>3</sub> alkanes)
<b>Aerosol Species<sup>2</sup></b>		
Sea Salt (0.03-0.5 micrometer)	Desert Dust (0.03-0.55 micrometer)	OM (organic matter)
Sea Salt (0.5-5 micrometer)	Desert Dust (0.55-0.9 micrometer)	BC (black carbon)
Sea Salt (5-20 micrometer)	Desert Dust (0.9-20 micrometer)	SO <sub>2</sub> (sulfur dioxide-gas) <sup>3</sup>
<b>Other Variables</b>		
T (temperature) <sup>4</sup>	PS (surface pressure) <sup>5</sup>	

676 <sup>1</sup>volume mixing ratios; units: mole mole<sup>-1</sup>

677 <sup>2</sup>units: μg m<sup>-3</sup>; size distribution bins are chosen so that roughly 10, 20 and 70 percent of the total mass of each  
 678 aerosol type are in the three successive bins

679 <sup>3</sup>SO<sub>2</sub> here is based on simple assumptions of emissions and prescribed loss; no active chemistry

680 <sup>4</sup>units: °K; used in conversion between molar and mass mixing ratios for gas-phase species

681 <sup>5</sup>units: Pa; used in conversion of model layer number to atmospheric pressure

682

683 Table 2. Boundary Concentration Data Sources Used by AQMEII Participants  
 684

<b>AQMEII Participant</b>	<b>Model System</b>	<b>Source of Boundary Concentration Data</b>
ZAMG - Austrian Weather Service - AT	ALADIN/CAMx	CECILIA model
Environment Canada - CA	GEM/AURAMS	Climatological chemical boundary concentrations with dynamic O <sub>3</sub> adjustments (Makar et al., 2010)
Paul Scherrer Institute - CH	WRF/CAMx	GEMS re-analysis
Leibniz Institute for Tropospheric Research - DE	COSMO	GEMS re-analysis
HZG Research Centre - DE	CCLM/CMAQ	GEMS re-analysis
University of Aarhus - DK	MM5v3/DEHM	DEHM hemispheric simulation
Barcelona Supercomputing Centre - ES	WRF/CMAQ/DREAM8b	GEMS re-analysis
Finnish Meteorological Institute - FI	ECMWF/SILAM	GEMS re-analysis
CEREA - FR	POLYPHEMUS	GEMS re-analysis
INERIS/IPSL - FR	CHIMERE	GEMS re-analysis; LMDzINCA model
Meteorological Service of Croatia - HR	EMEP/HIRLAM-PS	EMEP model
TNO - NL	LOTOS-EUROS	GEMS re-analysis
Kings College London - UK	WRF/CMAQ	STOCHEM model
University of Hertfordshire - UK	WRF/CMAQ	GEMS re-analysis; GEOS-Chem
Environmental Protection Agency - US	WRF/CMAQ	GEMS re-analysis
Environ Corporation - US	WRF/CAMx	GEMS re-analysis

685  
 686

687 Table 3. Standard deviation of daily means at the location of surface air quality monitoring  
688 stations for O<sub>3</sub>, NO<sub>2</sub> and PM10 in the data and in the two CHIMERE model simulations (3HR  
689 and CST).  
690  
691

	Obs. data	3HR	CST
O <sub>3</sub> (µg/m <sup>3</sup> )	26.17	21.67	21.26
NO <sub>2</sub> (µg/m <sup>3</sup> )	16.48	13.11	13.12
PM10 (µg/m <sup>3</sup> )	22.75	24.11	23.93

692  
693

694 **Figure Captions**

695

696 **Fig 1.** Schematic of the components of the GEMS modeling system (figure provided courtesy of  
697 M.G. Schultz, FZ-Jülich).

698

699 **Fig. 2.** Timeline of satellite data usage for variables used in the GEMS re-analysis. AQMEII  
700 modeling is focused on 2006.

701

702 **Fig. 3.** Domain cut-outs from global GEMS re-analysis grid used for providing boundary  
703 concentrations for (a) Europe and (b) North America.

704

705 **Fig. 4.** Time series of May – September average daily maximum 1-h O<sub>3</sub> concentrations for  
706 observations and two sets of CMAQ simulations. CMAQ/Profile refers to the CMAQ  
707 simulations utilizing time-invariant climatological vertical profiles for the specification of  
708 boundary conditions while CMAQ/Global refers to the CMAQ simulations utilizing boundary  
709 conditions derived from a global chemistry model. The time series represent spatial averages  
710 over the location of all O<sub>3</sub> monitors in the modeling domain. Further details on these simulations  
711 are provided in Hogrefe et al. (2011).

712

713 **Fig. 5.** Locations of IONS-2006 North American ozonesonde launch sites within the CMAQ  
714 modeling domain. Shaded area represents the analysis region for inflow air from the western  
715 boundary of the domain.

716

717 **Fig. 6.** Mean O<sub>3</sub> concentrations for (a) March 2006 and (b) August 2006 for vertical profiles at  
718 Trinidad Head, California (US). Observed mean concentrations (with standard deviations) are  
719 indicated by gray circles; CMAQ mean concentrations are indicated by open circles; boundary-  
720 tracer concentrations are indicated by triangles.

721

722 **Fig. 7.** Fractional contribution of the boundary conditions to the simulated mean vertical O<sub>3</sub>  
723 distributions during March and August 2006 at Trinidad Head.

724

725 **Fig. 8.** Same as Fig. 5, except for Kelowna, British Columbia (Canada).

726

727 **Fig. 9.** Vertical profiles from the GEMS re-analysis database of primary organic particulate  
728 matter (OM) along each boundary of the CMAQ model North American domain averaged over  
729 the period of 21-30 June 2006.

730

731 **Fig. 10.** CMAQ model-predicted average primary organic aerosol on 30 June 2006 at 01 UTC  
732 using GEMS boundary concentrations.

733

734 **Fig. 11.** Mean seasonal distribution for 2006 of the difference of surface O<sub>3</sub> concentration  
735 between the CHIMERE simulation using the LMDzINCA (gas phase) and GOCART (aerosols)  
736 boundary conditions and that using the GEMS boundary conditions. Concentration differences  
737 are in ppb. The horizontal resolution of the simulations is 36 km. Each panel corresponds to a  
738 seasonal mean.

739

740 **Fig 12.** Seasonal mean of the bias in modeled O<sub>3</sub> (ppb) at the surface in the CHIMERE model:  
741 difference between the simulation driven by 3-hourly boundary conditions and the monthly  
742 climatology, JFD (January, February, December), MAM (March, April, May), JJA (June, July,  
743 August), SON (September, October, November).

744  
745 **Fig. 13.** Difference in standard deviation of modeled O<sub>3</sub> (left, ppb) and PM10 (right, μg/m<sup>3</sup>) at  
746 the surface in the CHIMERE model between the simulation driven by 3-hourly BCs and when a  
747 monthly climatology is used at the boundaries.

748  
749 **Fig 14.** Vertical distribution of O<sub>3</sub> at Lerwick, Shetland Mainland, UK, for the year 2006 as (a)  
750 observed, (b) simulated with CMAQ model using the GEMS boundary concentrations, and (c)  
751 simulated with CMAQ model using the GEOS-Chem boundary concentrations.

752  
753 **Fig. 15.** Time series of observed (black) and CMAQ-simulated (colors) 1-h O<sub>3</sub> concentrations at  
754 Mace Head, Republic of Ireland, for the year 2006 for (a) the simulation using the GEMS  
755 boundary concentrations and (b) that using the GEOS-Chem boundary concentrations. Color  
756 variations in simulated time series represents different seasons.

757  
758

Figure 1

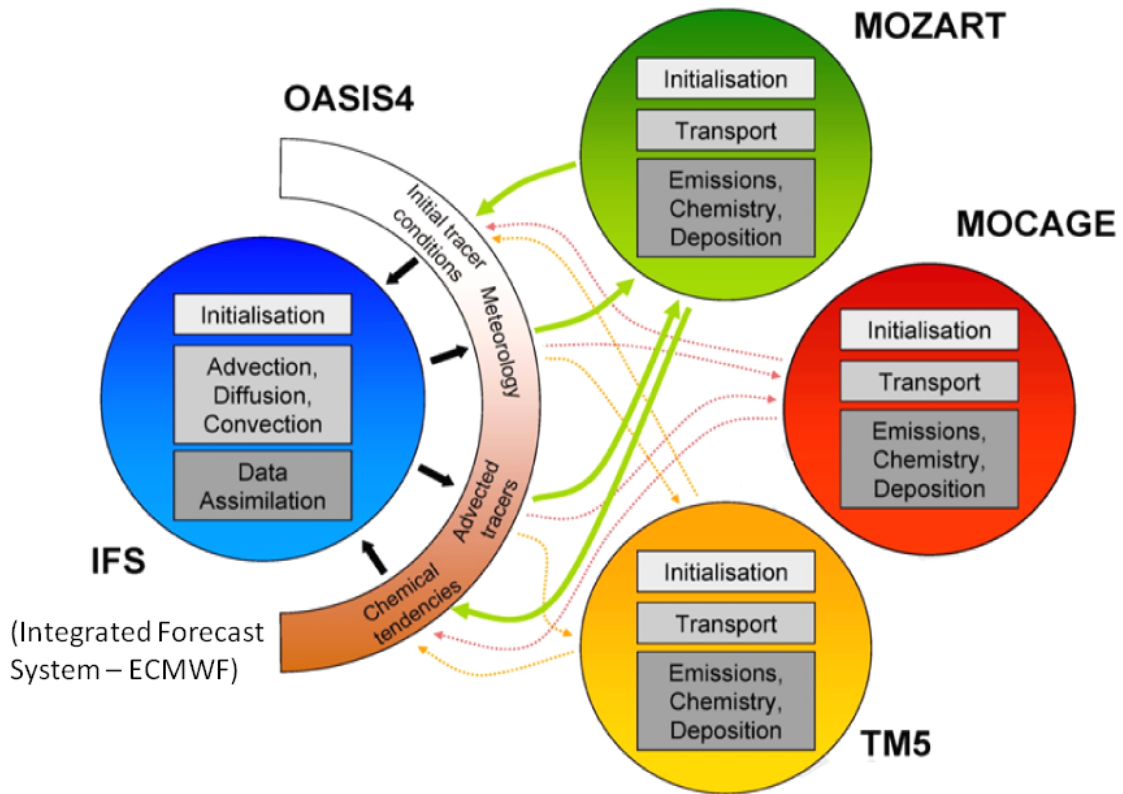


Figure 2

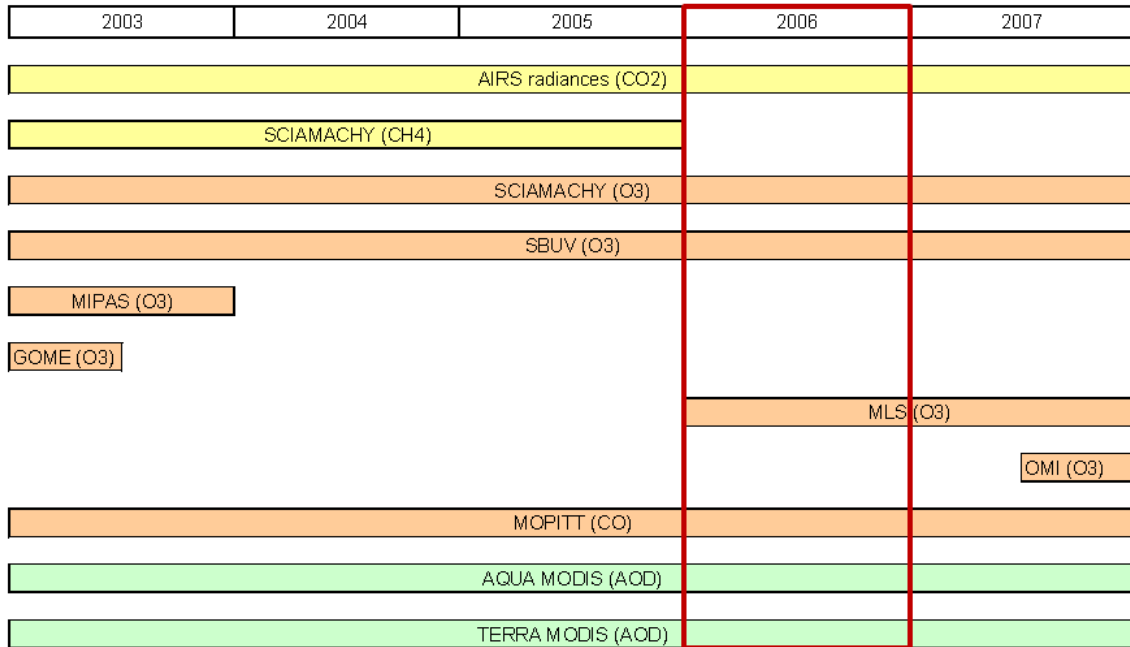


Figure 3 (a)

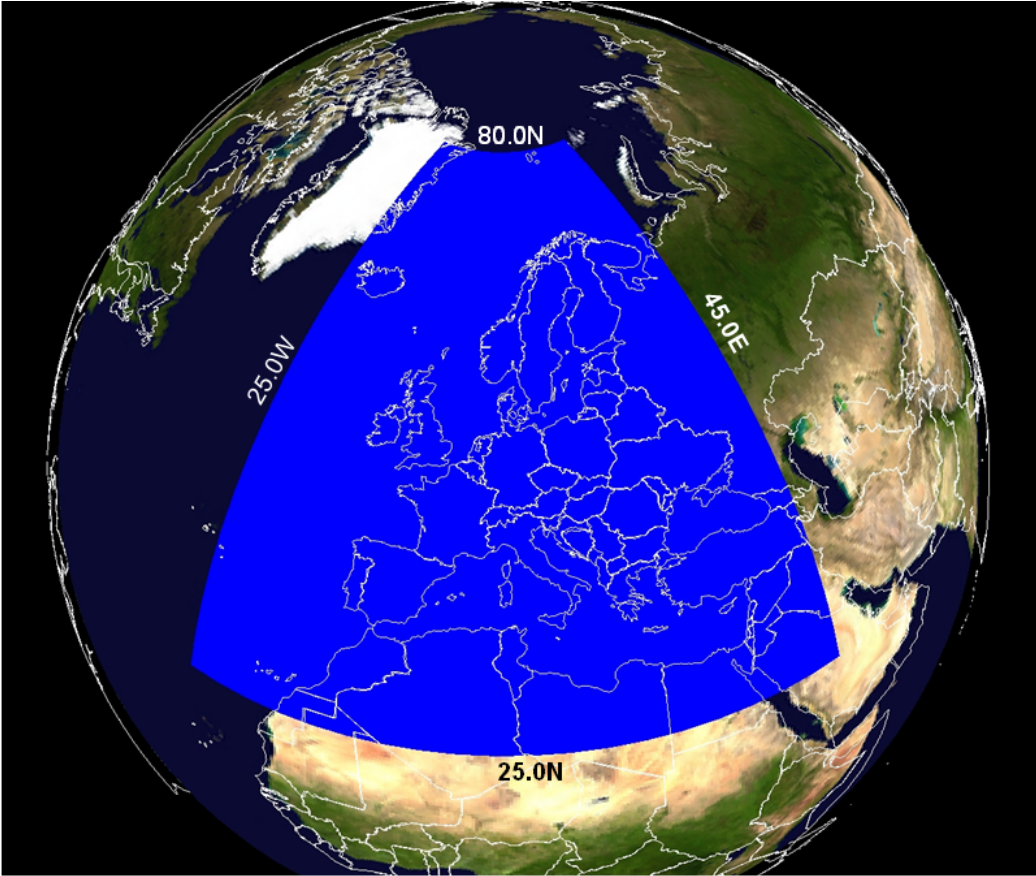


Figure 3b



Figure 4.

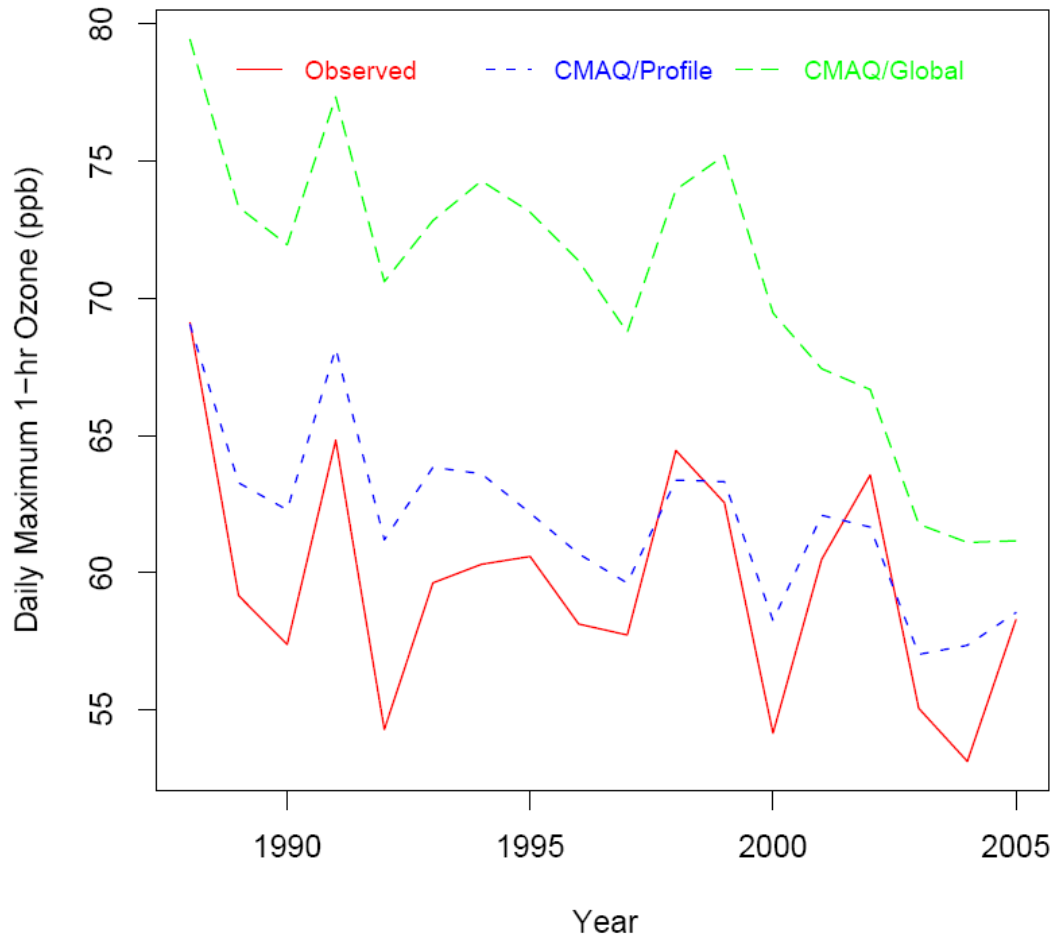


Figure 5

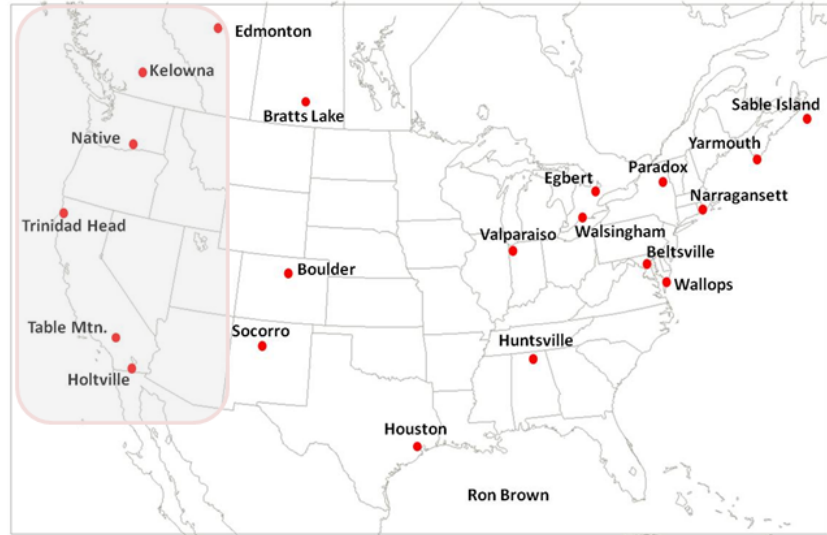


Figure 6a

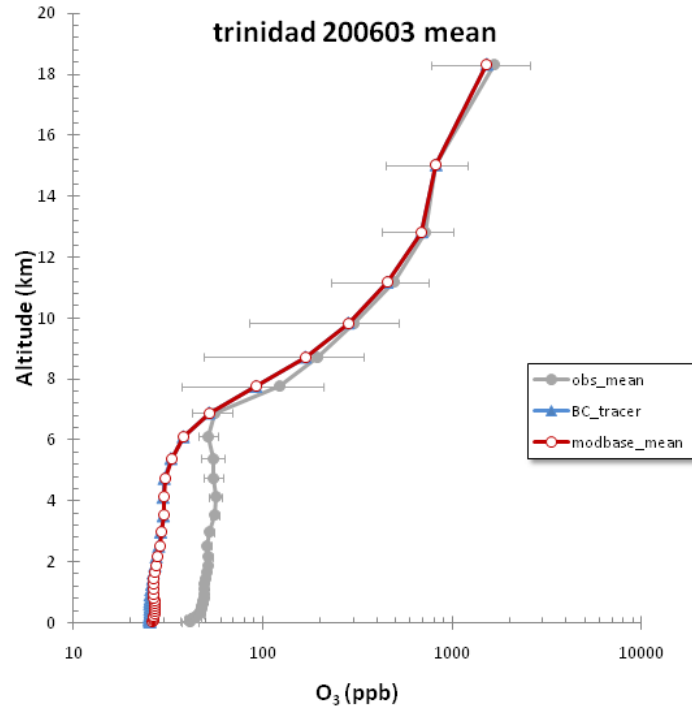


Figure 6b

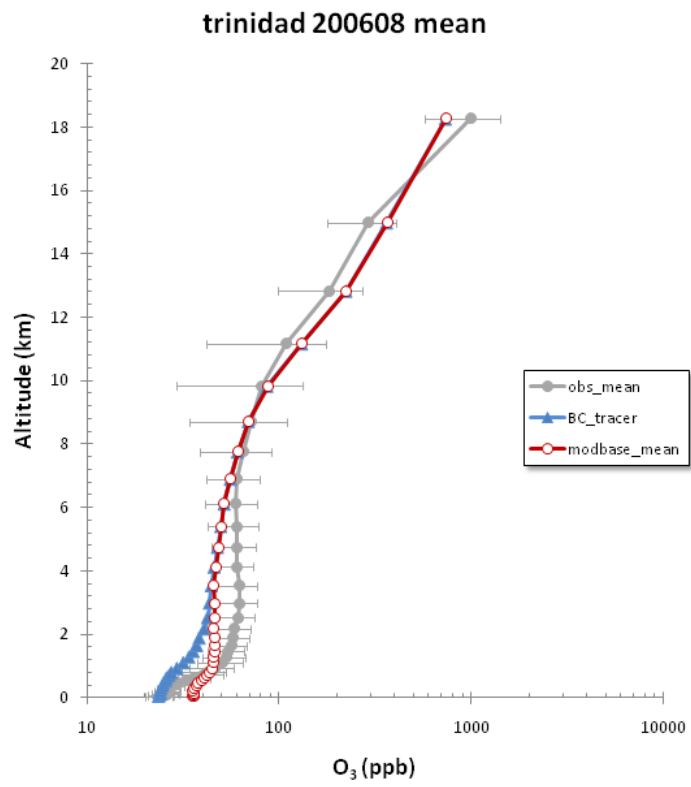


Figure 7

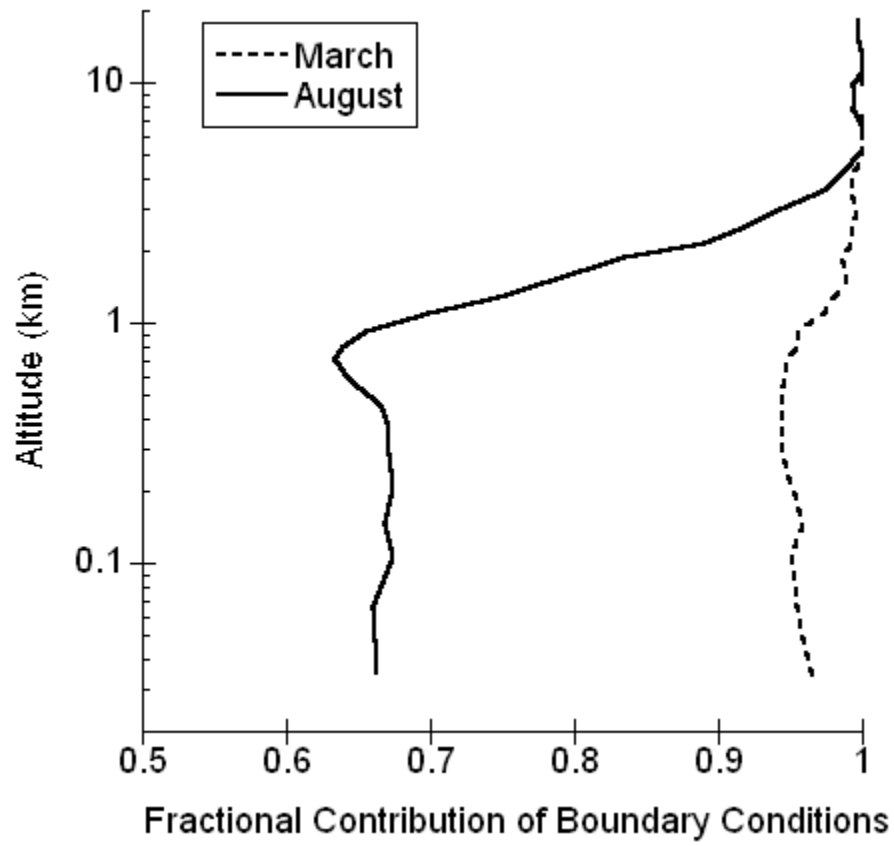


Figure 8a

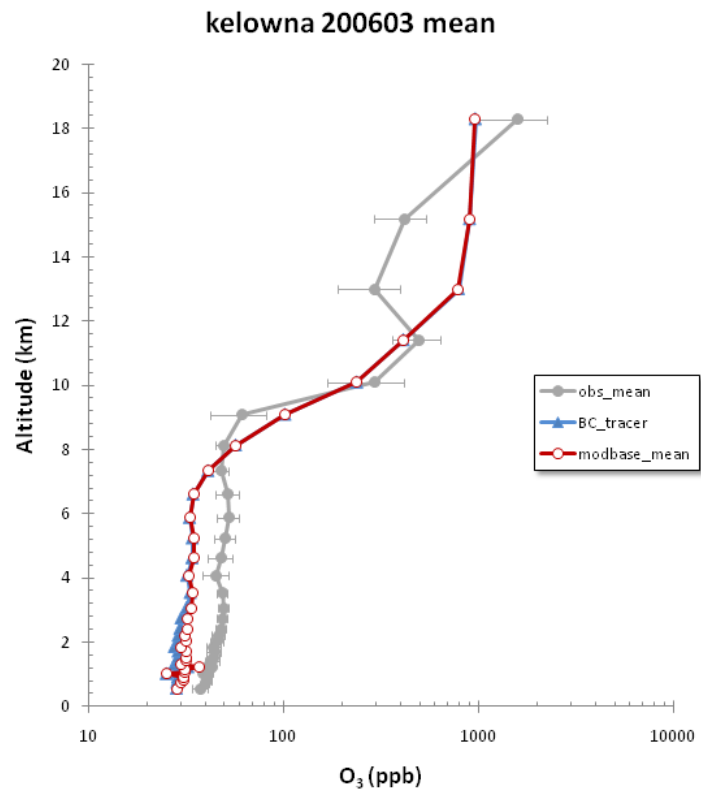


Figure 8b

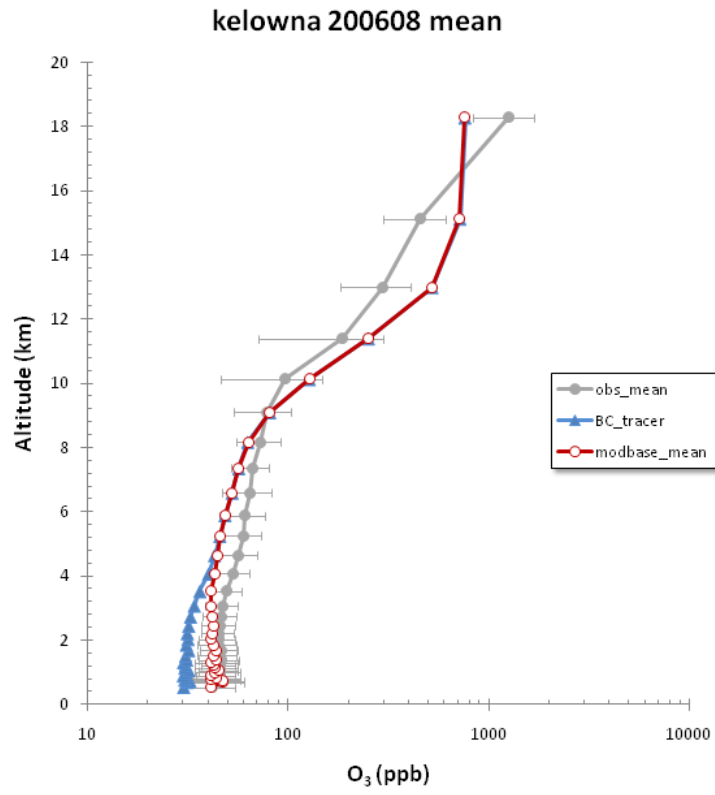


Figure 9

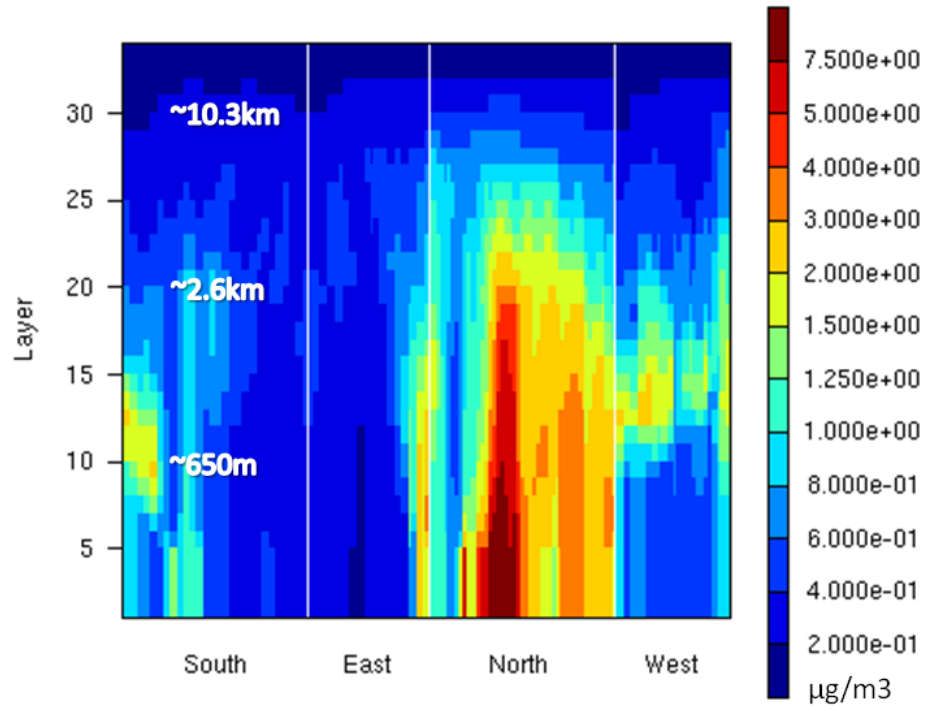


Figure 10

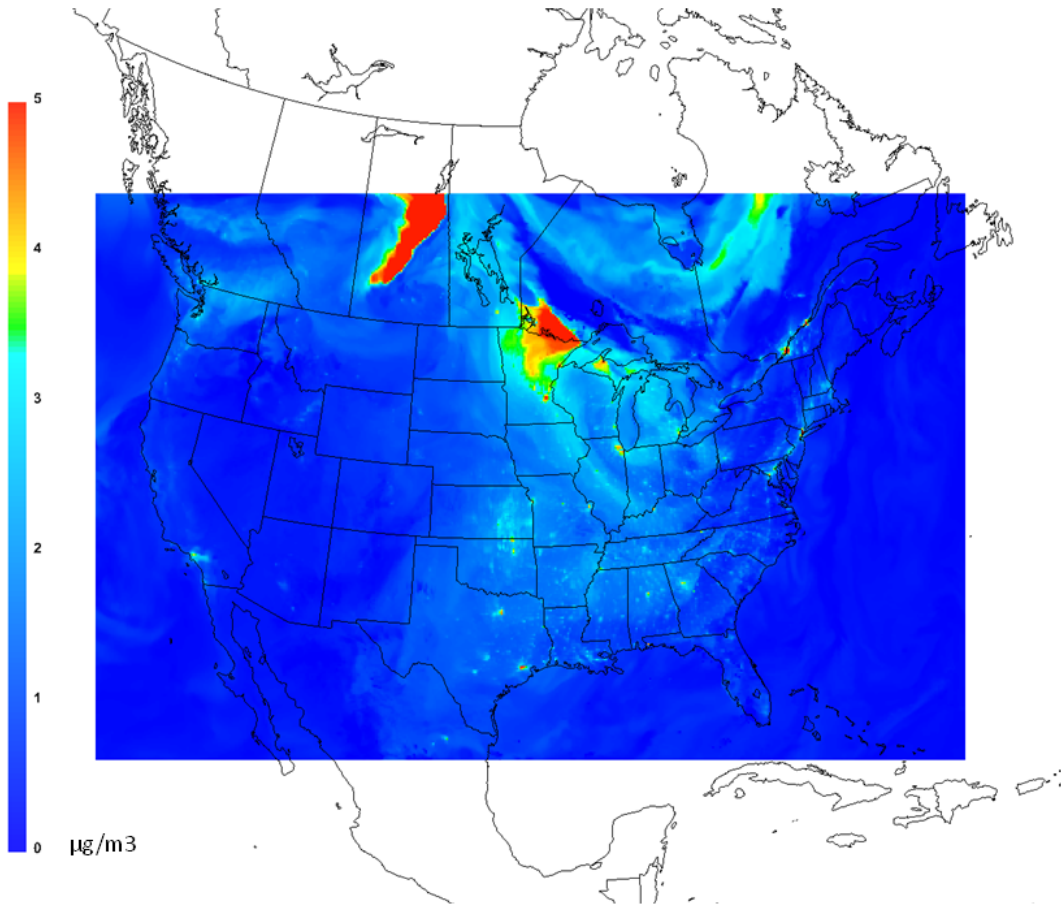


Figure 11

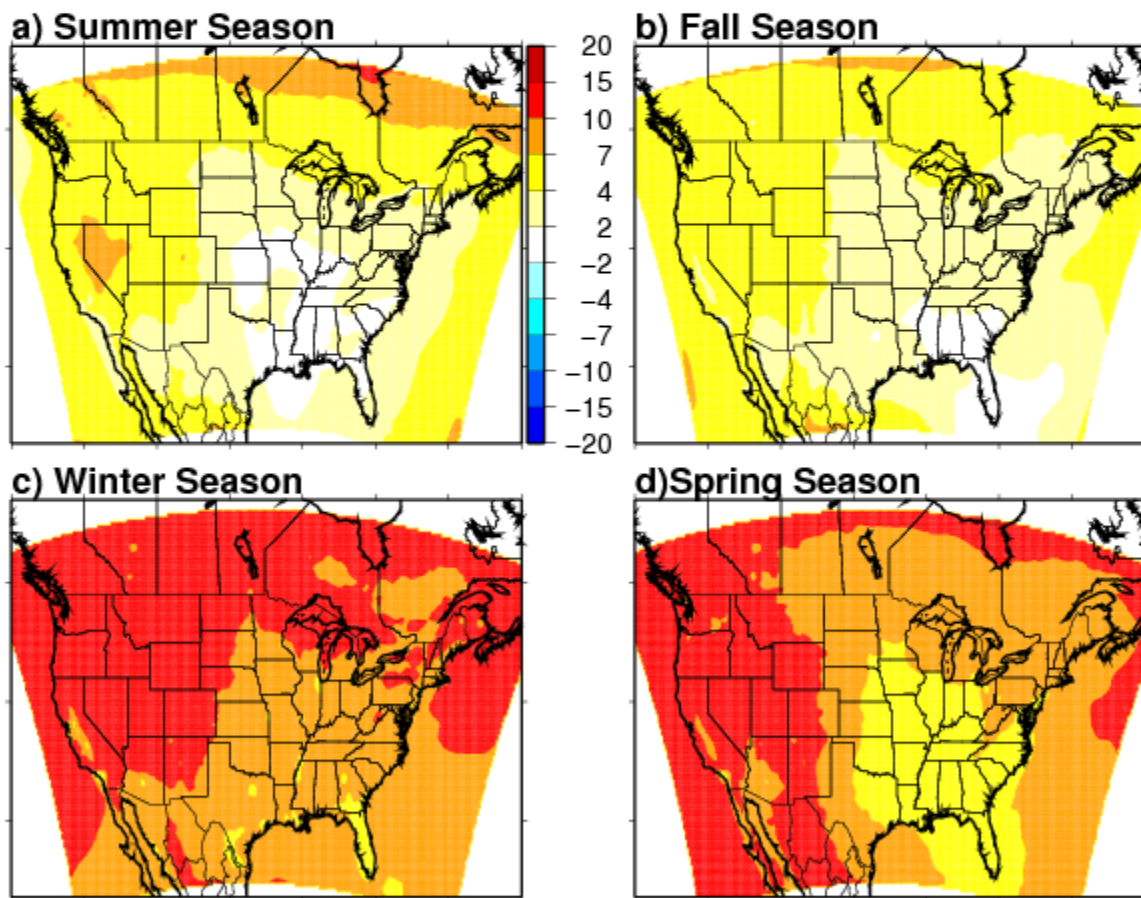


Figure 12.

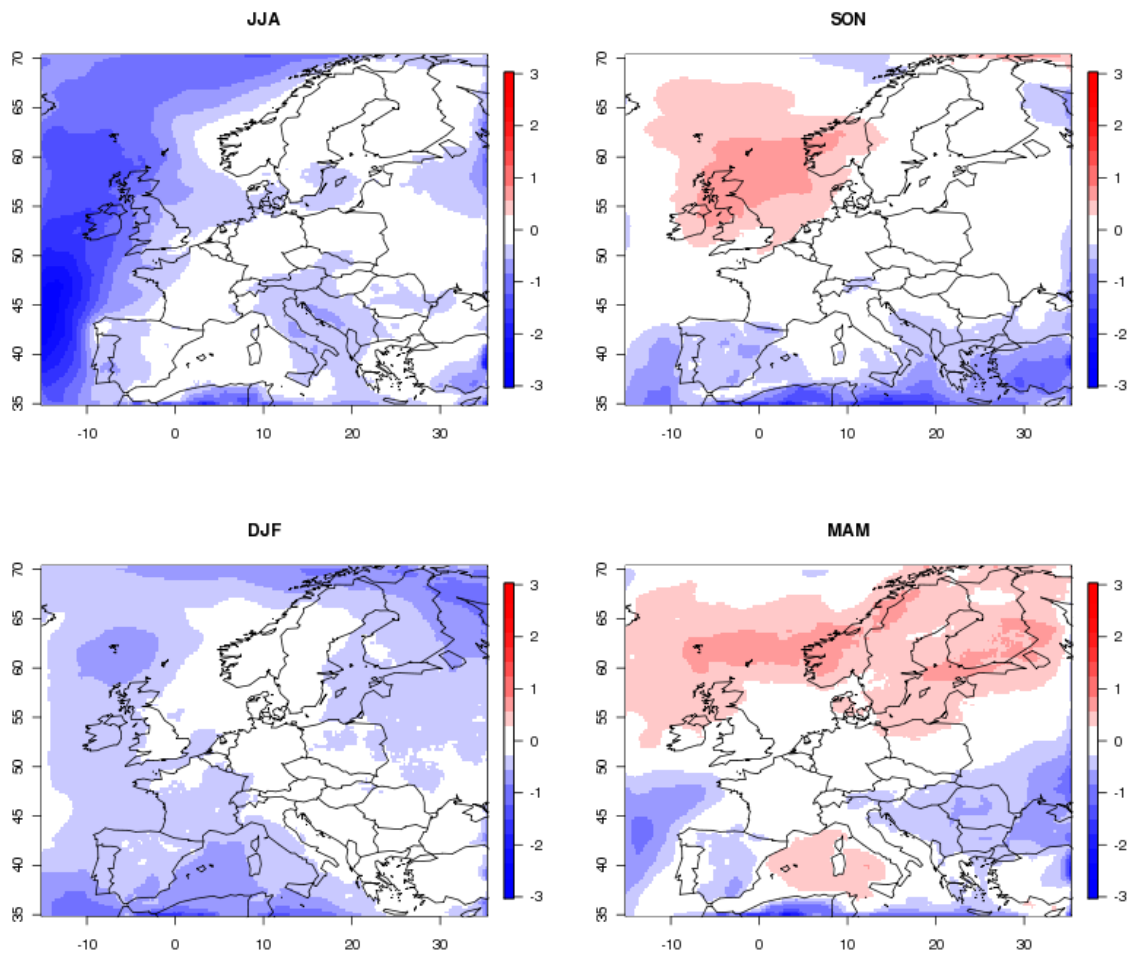


Figure 13.

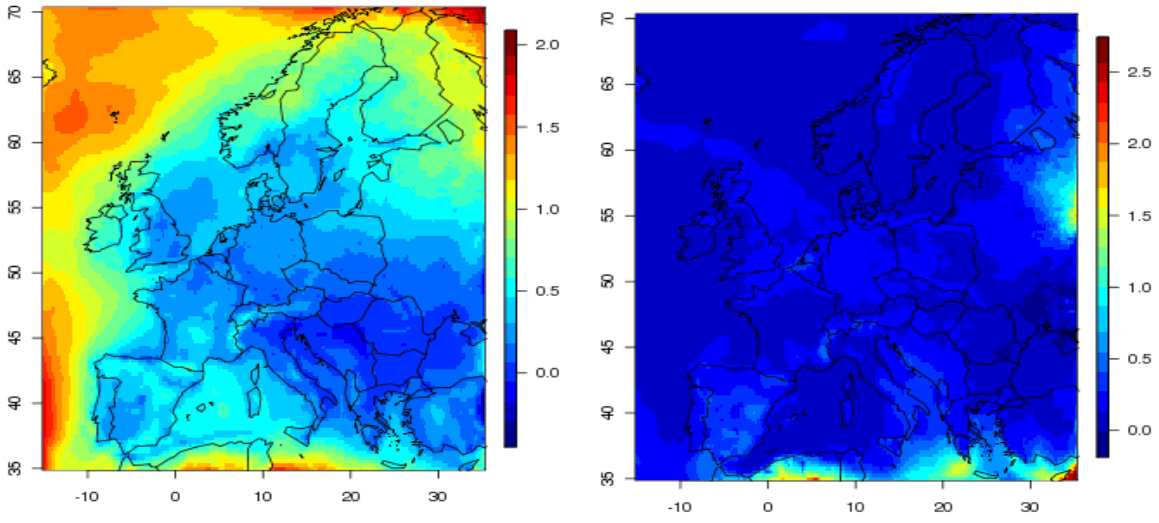


Figure 14.

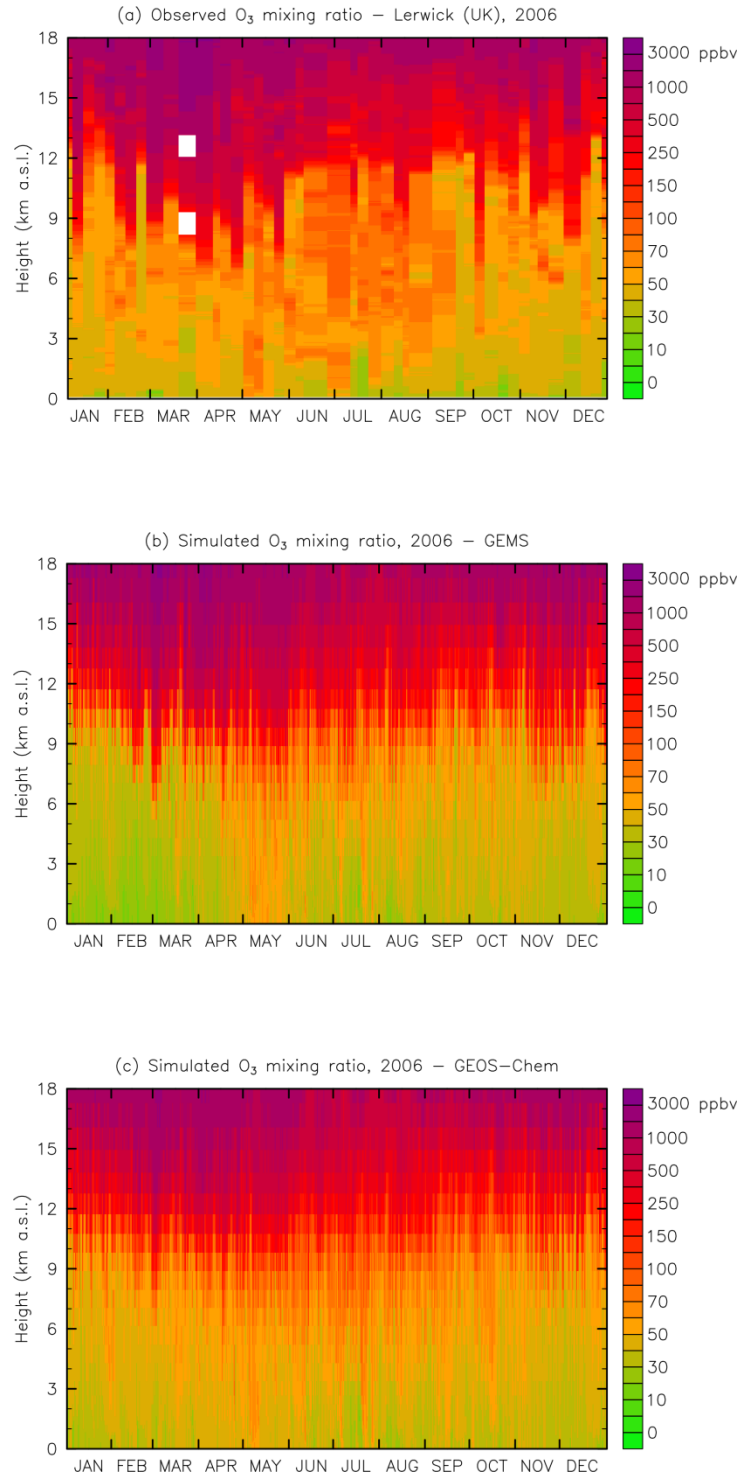


Figure 15.

